Nonlinear mixture models for analyzing laboratory simulated-forest hyperspectral data

Javier Plaza*, Antonio Plaza, Pablo Martínez, Rosa Pérez
Neural Networks and Signal Processing Group (GRNPS), Computer Science Department,
University of Extremadura, Avda. de la Universidad S/N, 10071 Cáceres, SPAIN.

ABSTRACT

The interpretation of mixed pixels is a key factor in the analysis of hyperspectral imagery. A commonly used approach to mixed pixel classification has been linear spectral unmixing. However, the question of whether linear or nonlinear processes dominate spectral signatures of mixed pixels is still an unresolved matter. In this paper we describe new methodologies for inferring land cover fractions within hyperspectral scenes, using nonlinear mixture modeling techniques based on support vector machines and neural network-based techniques. A comparative analysis of these mixture estimation methods to the standard linear mixture model has been carried out using a database of laboratory simulated-forest scenes. For the simulations, canopies of both opaque and translucent trees were simulated using objects mounted on stems. Two tree densities (sparse and dense) and three background colors (dark, white and green) were considered. Hyperspectral images of these simulated scenes were acquired by the Compact Airborne Spectrographic Imager (CASI), and the areal fractions of the main constituents calculated by the SPRINT canopy model were used for comparison. Our quantitative and comparative analysis reveals that nonlinear approaches outperform linear mixture model-based approaches, particularly in the scenes with translucent trees. As a result, this investigation suggests that nonlinear mixture models are needed to account for the multiple scattering between tree crowns and background for the laboratory simulated-forest scenes used in this study.

Keywords: Nonlinear mixture models, Laboratory simulated-forest data, Support vector machines.

1. INTRODUCTION

During the recent years, several different methodologies have been developed for hyperspectral image analysis and classification. The interpretation of mixed pixels is a key factor in the analysis of hyperspectral imagery. Mixed pixels are a mixture of more than one distinct substance, and exist for one of two reasons. Firstly, if the spatial resolution of the sensor is not high enough to separate different materials, these can jointly occupy a single pixel, and the resulting spectral measurement will be a composite of the individual spectra. Secondly, mixed pixels can also result when distinct materials are combined into a homogeneous mixture. This circumstance occurs independent of the spatial resolution of the sensor. A commonly used approach to mixed pixel classification has been linear spectral unmixing, which uses a linear mixture model (LMM) to estimate the abundance fractions of spectral signatures within a mixed pixel. Although LMM has been demonstrated in numerous applications to be a useful technique for interpreting remote sensing data with high dimensionality, the question of whether linear or non-linear processes dominate spectral signatures of mixed pixels is still an unresolved matter[1]. It has been reported that the reflectance spectrum of a mixture is a systematic combination of the component reflectance spectra in the mixture[2]. The systematics are linear if components of interest in a pixel appear in spatially segregated patterns. If, however, the components are in intimate association, light typically interacts with more than one component as it is multiply scattered, and the mixing systematics between the different components are highly nonlinear. These nonlinear effects are an area of active research in particular applications as vegetation and canopy studies[3], where LMM generally result in poor mixture analysis accuracy. As demonstrated in previous work, non-linear mixture models can achieve much higher accuracy[4,5].

In this paper, we investigate new methodologies for inferring land cover fractions within hyperspectral scenes. The proposed methods are based on data selection procedures through support vector machines (SVM), which are based on the principle of optimal class separation[6]. The use of such methods is motivated in part by the recent profusion of high-

* E-mail: jplaza@unex.es; Phone: +34 927257254; Fax: +34 927257203.

Image and Signal Processing for Remote Sensing IX, edited by Lorenzo Bruzzone, Proceedings of SPIE
Vol. 5238 (SPIE, Bellingham, WA, 2004) · 0277-786X/04/$15 · doi: 10.1117/12.511127

dimensional methods in remote sensing, where hyperspectral sensors measure radiance at hundreds of contiguous channels for each ground pixel. For these data, part of the challenge is for classifiers that perform well in such high-dimensional spaces. In previous work, it has been demonstrated that the constrained least squares LMM is equivalent to the linear SVM[7]. This fact reveals that the LMM algorithm can be derived from the same optimality conditions as the linear SVM. In addition, extensions to the basic SVM algorithm allow the technique to be applied to datasets that exhibit spectral confusion (overlapping sets of pure pixels) and to datasets that have nonlinear mixture regions. Such regions can be described using kernels such as radial basis functions, polynomials and sigmoid nodes[6]. In each case, the input space is mapped to a higher dimensional "kernel space" and the same processes are performed in this transformed space. The range of different kernel nodes include traditional nonlinear modeling algorithms as well as some neural network-based techniques[7].

In this work, a comparative analysis of SVM-based mixture estimation methods to the standard constrained least squares LMM has been carried out using a database of laboratory simulated-forest scenes. It should be taken into account that the generation of reliable ground-truth in real scenarios is difficult and expensive. The amount of hyperspectral datasets with quality ground measurements for public use is very limited, a fact that has largely prevented the existence of comparative surveys using large databases of real images. In order to avoid the previously addressed shortcoming, several authors have used simulated imagery as a simple and intuitive way to perform a preliminary evaluation of hyperspectral analysis techniques. The primary reason for the use of simulated imagery in this work is that all details of the constructed images are known. These details, which include spectral mixing, scene geometry and the spatial relationships and physical properties of objects, can be efficiently investigated because they can be manipulated individually and precisely. As a result, the performance of spectral mixture analysis algorithms can be examined in a controlled manner.

The remainder of the paper is organized as follows. In section 2, the proposed SVM-based techniques for nonlinear abundance estimation in hyperspectral analysis are described. Section 3 describes the laboratory-simulated data used in the present study. Section 4 presents a comparative performance analysis for the algorithms described in section 2. Section 5 concludes with some remarks.

2. SUPPORT VECTOR MACHINES FOR ABUNDANCE ESTIMATION

Support Vector Machines (SVMs) are classification methods which are based on the principle of "optimal separation," where if the classes are separable, the solution is chosen which maximally separates the classes[6]. In this work, this process is based on the consideration of pure pixels (exemplars) as support vectors, i.e. those lying on the class boundary. Next, we provide an overview of linear and nonlinear SVM techniques used in this work for the purpose of abundance estimation in hyperspectral imagery.

2.1. Linear SVMs

Linear SVMs use linear discrimination models to separate classes which are linearly separable. Hence, in applying a linear SVM for pure pixel discrimination, it is assumed that the problem has two classes, and that the data can be linearly separated. The task is then to find the linear discriminator which maximally separates the classes. Although in our problem we will assume that the output of an SVM lies in the unit interval $[0,1]$, for the purposes of deriving the algorithms it is more convenient to assume, without loss of generality, that the output lies in the bipolar interval $[-1,1]$. Given a training set of instance-label pairs $(\boldsymbol{x}_i, \boldsymbol{y}_j)$, $i = 1, 2, ..., l$, where the $\boldsymbol{x}_i \in R^n$ are hyperspectral image pixels which are used as exemplars of either a "pure" class, i.e. $\boldsymbol{y}_j = 1$, or "non-pure" class, i.e. $\boldsymbol{y}_j = -1$. It is assumed that no spectral confusion is present in the data, so the aim is to maximize the size of the mixing margin such that all the data are correctly labeled as either 1 or –1. This can be specified as the following optimization problem[8]:

$$\begin{aligned} &\text{Minimize } \|\boldsymbol{w}\|_2^2, \\ &\text{subject to } \left(\boldsymbol{w}^T \Phi(\boldsymbol{x}_i) + b\right)\boldsymbol{y}_j \geq 1 \qquad i = 1, 2, ..., l, \end{aligned} \tag{1}$$

where $\boldsymbol{w}$ is the weight vector for the model, which describes the orientation of the margin and boundaries, and b is a bias term. Here training vectors $\boldsymbol{x}_i$ are mapped into a higher dimensional space by the function Φ. As shown in (1), the first

constraint minimizes the size of the weight vector (maximizes the margin's size) in order to separate the data optimally. Fig. 1 illustrates the performance of linear SVMs by showing a scatter plot of two uncorrelated spectral bands of a multispectral scene. Two potential mixing margins for a two-input, two-class problem with pure pixels $\boldsymbol{x}_1$ and $\boldsymbol{x}_2$ are shown in the figure. The solid lines denote the boundaries for the solution which maximize the margin's width. The dashed lines are also a potential solution.

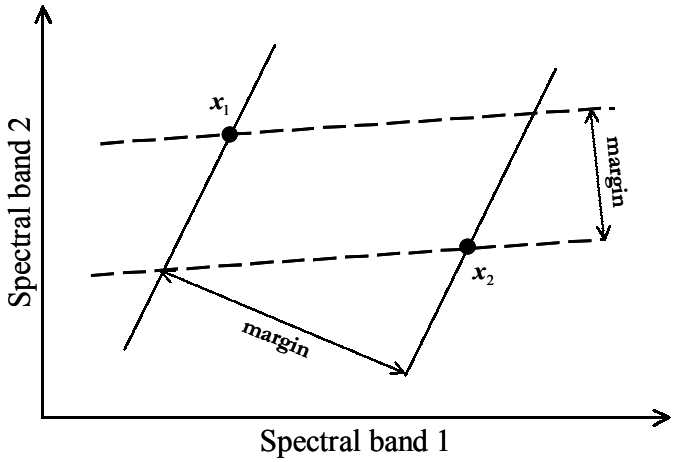

Figure 1. Two linear SVM solutions for a two-input, two-class problem in multispectral data.

In previous work[8], it has been demonstrated that the linear SVM is equivalent to the constrained least squares LMM. In such work, it was shown that the two calculated weight vectors by the two models are identical. However, it should be taken into account that the SVM approach is not limited to simply linear decision boundaries as kernel-based, nonlinear mappings can be used to construct more flexible decision boundaries.

2.2. Nonlinear SVMs

In the design of nonlinear SVMs, all of the previous analysis holds for forming the decision boundary. The only change that needs to be made is to incorporate a kernel function[9], which is denoted in this work by

$$\mathrm{K}(\boldsymbol{x}_\mathrm{i}, \boldsymbol{x}_\mathrm{j}) \equiv \Phi(\boldsymbol{x}_\mathrm{i})^\mathrm{T} \Phi(\boldsymbol{x}_\mathrm{j}). \tag{2}$$

Then, instead of performing the data selection in the original feature space, a higher dimensional, nonlinear transformation is used. This is the purpose of the kernel functions: to map the data into an alternative space in which the problem may be linearly separable. Common choices for the kernel functions include the following[9].

- Linear: $\mathrm{K}(\boldsymbol{x}_\mathrm{i}, \boldsymbol{x}_\mathrm{j}) \equiv \boldsymbol{x}_\mathrm{i}^\mathrm{T} \boldsymbol{x}_\mathrm{j}$.
- Polynomial: $\mathrm{K}(\boldsymbol{x}_\mathrm{i}, \boldsymbol{x}_\mathrm{j}) \equiv (\boldsymbol{x}_\mathrm{i}, \boldsymbol{x}_\mathrm{j} + 1)^\mathrm{d}, \mathrm{d} = 1, 2, ..., \mathrm{N}$.
- Radial basis function (RBF): $\mathrm{K}(\boldsymbol{x}_\mathrm{i}, \boldsymbol{x}_\mathrm{j}) \equiv \exp\left(- \left\| \boldsymbol{x}_\mathrm{i} - \boldsymbol{x}_\mathrm{j} \right\|^2 \right)$.
- Sigmoid: $\mathrm{K}(\boldsymbol{x}_\mathrm{i}, \boldsymbol{x}_\mathrm{j}) \equiv \tanh(\mathrm{b}(\boldsymbol{x}_\mathrm{i} - \boldsymbol{x}_\mathrm{j}) - \mathrm{c})$, for certain values of b, c.

Various nonlinear mixture models have been proposed in the literature, including neural network-based approaches[7] and polynomial transformations[8]. By extending the linear SVM model to include nonlinear kernels, all of the previously addressed techniques apply to implementing approaches for dealing with separable and nonseparable mixtures in hyperspectral imagery. It should be taken into account that these approaches are subject to the "curse of dimensionality," which refers to the exponential increase in data and model resources required to deal with feature space complexity as the number of inputs increases. In this regard, nonlinear mappings are more flexible than linear approaches.

So far, the mixture-modeling problem has been posed as finding an algorithm which models regions of pure pixels, i.e. data are labeled with a 1 (to denote an exemplar pure pixel) or a 0 (to denote a pure pixel which is not a member of that class). However, remotely sensed data is dominated by examples of mixed data, where the target values lie in the interval $[0,1]$ and conform to the sum to unity assumption. Often, it is difficult to identify single pure pixels in the data, so techniques need to be developed which can make use of large hyperspectral datasets containing mixed pixels. In the literature, it has been reported that it is possible to extend the SVM algorithms to an scenario dominated by mixed pixels[8]. The models that can be used are identical to those ones used for classification, so they can be linear or use any of the above nonlinear kernel functions. In this work, we achieve the above goal by using exemplar data based on actual mixtures, thus allowing the proposed linear and nonlinear schemes to adapt to the mixing scenario. This is a flexible approach, which requires that the empirical, sampled dataset is representative of how the model will be applied.

3. LABORATORY SIMULATED-FOREST HYPERSPECTRAL DATA

A database of laboratory-simulated scenes has been developed at CRESTech (Center for Research in Earth and Space Technology) to investigate nonlinear effects in simulated natural forest landscapes[10]. Two kinds of objects, opaque and translucent, were mounted on stems to simulate forest crowns on trunks. The dimensions of tree crowns for opaque and translucent trees ranged from 1.3 cm to 1.7 cm. These simulated trees were randomly placed on a 40 cm by 40 cm mounting board covered with different backgrounds: dark, green and white. Canopies of both opaque and translucent trees were designed, with two different tree densities: sparse and dense. For the sparse canopies, 40 trees were planted in the mounting board, while 100 trees were used for the dense canopies. Scene illumination was generated using a 100 W tungsten lamp and illumination angle of 40º. Hyperspectral images of these simulated forest scenes were acquired by the Compact Airborne Spectrographic Imager (CASI), a pushbroom imager, by moving the entire scene perpendicularly at a constant rate with respect to the CASI field-of view[10]. The hyperspectral CASI images were acquired in 72 spectral channels covering the spectral region from 414 to 914 nm, at a nominal spectral resolution of 7.5 nm. The main properties of the 12 scenes, labeled as CASI01_01..CASI01_12, are summarized in Table 1. For illustrative purposes, Fig. 2 shows a picture of the twelve simulated scenes, along with representative spectral signatures of the main constituents present in some of the scenes. The areal fractions of ground constituents in these scenes were calculated by the SPRINT canopy model[11], which uses the concept of ray-tracing and Monte Carlo simulation. Table 2 shows the areal fractions calculated by the SPRINT model, that will be used as ground-truth in the present study. As shown in Fig. 2, the images are formed by three different constituents, i.e. sunlit tree, sunlit background and shadow.

Scene	Size in pixels	Background	Tree population	Type of trees
CASI01_01	148x216	Green	Sparse	Opaque
CASI01_02	148x185	Green	Sparse	Translucent
CASI01_03	148x192	Green	Dense	Opaque
CASI01_04	148x203	Green	Dense	Translucent
CASI01_05	148x204	White	Sparse	Opaque
CASI01_06	148x184	White	Sparse	Translucent
CASI01_07	149x186	White	Dense	Opaque
CASI01_08	148x207	White	Dense	Translucent
CASI01_09	148x200	Dark	Sparse	Opaque
CASI01_10	148x178	Dark	Sparse	Translucent
CASI01_11	148x200	Dark	Dense	Opaque
CASI01_12	148x213	Dark	Dense	Translucent

Table 1. Properties of laboratory simulated-forest hyperspectral scenes.

Scene	Tree	Background	Shadow
CASI01_01, CASI01_05, CASI01_09	0.109	0.723	0.167
CASI01_02, CASI01_06, CASI01_10	0.104	0.701	0.194
CASI01_03, CASI01_07, CASI01_11	0.294	0.383	0.318
CASI01_04, CASI01_08, CASI01_12	0.279	0.357	0.362

Table 2. Areal fractions obtained by the SPRINT model for laboratory simulated-forest hyperspectral scenes.

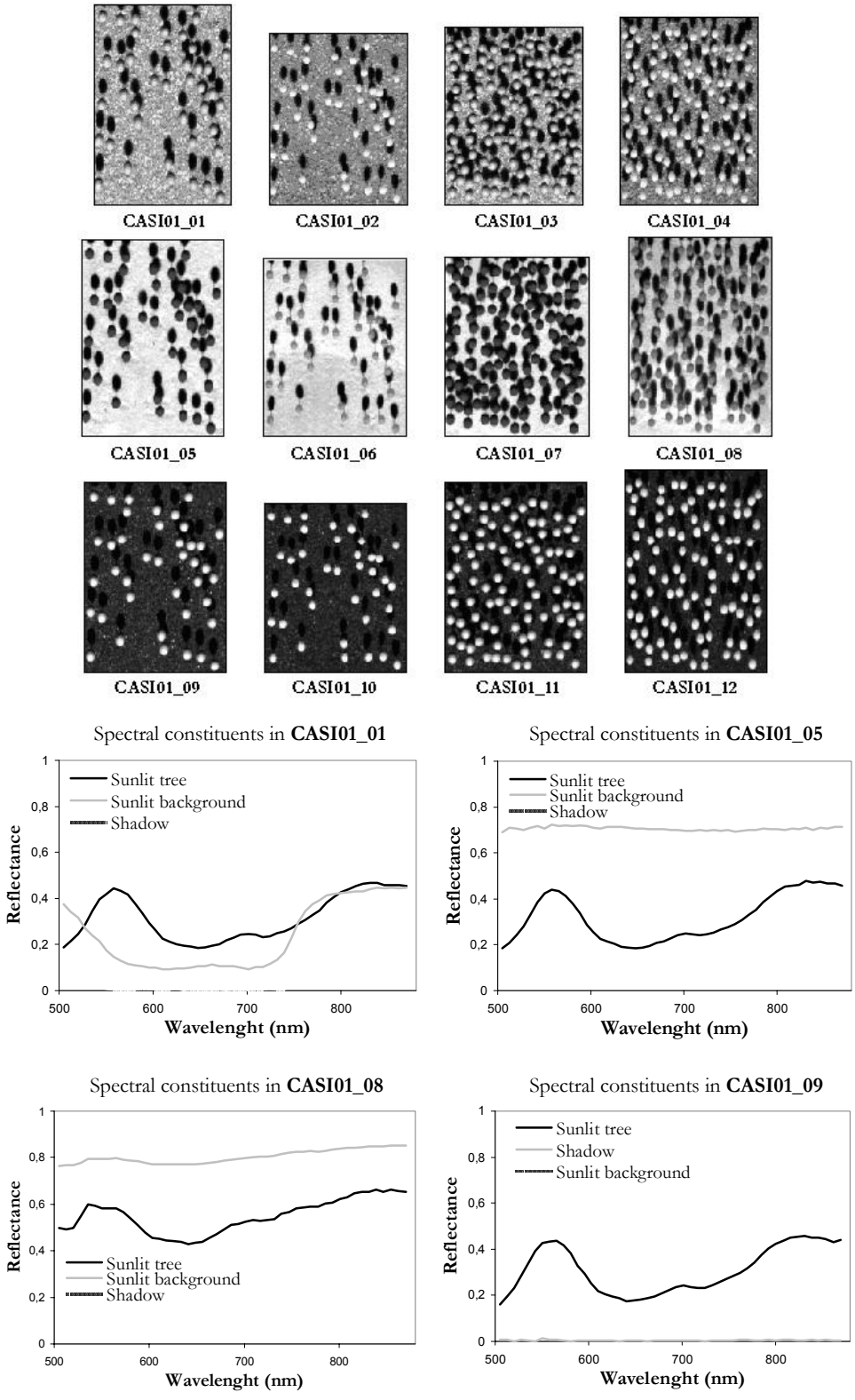

Figure 2. Visual description of laboratory simulated-forest hyperspectral data and representative spectral signatures of the main constituents found in some of the scenes.

4. RESULTS AND DISCUSSION

This section contains a series of experiments which use laboratory simulated-forest hyperspectral data to conduct a comprehensive comparison among linear and nonlinear spectral unmixing algorithms. One reason to limit our work to simulated data only is simply that developing a comparative framework for this problem seemed ambitious enough for a first step. Prior to a full examination and discussion of the results obtained, it is important that we first outline how these results will be presented and some of the assumptions used in the statistical analysis. Both the linear and nonlinear SVMs used in this study have been carefully trained using both pure and mixed data obtained from the laboratory simulated-forest scenes. To validate the results obtained using the linear and nonlinear SVM spectral unmixing approaches, the fractions of sunlit tree, sunlit background and shadow were compared to those found by the SPRINT model, as shown in Tables 3-6.

	Linear kernel			Polynomial kernel			RBF kernel			Sigmoid kernel		
Scene	Tree	Backg.	Shadow	Tree	Backg.	Shadow	Tree	Backg.	Shadow	Tree	Backg.	Shadow
CASI01_01	0.013	0.854	0.131	0.143	0.658	0.197	0.181	0.608	0.210	0.046	0.710	0.242
CASI01_05	0.036	0.888	0.074	0.063	0.665	0.271	0.121	0.669	0.209	0.158	0.681	0.160
CASI01_09	0.012	0.858	0.013	0.085	0.788	0.125	0.080	0.771	0.147	0.079	0.556	0.364
SPRINT model	0.109	0.723	0.167	0.109	0.723	0.167	0.109	0.723	0.167	0.109	0.723	0.167

Table 3. Estimated fractional covers obtained by the linear and nonlinear SVM-based models for the scenes with opaque trees and sparse population.

	Linear kernel			Polynomial kernel			RBF kernel			Sigmoid kernel		
Scene	Tree	Backg.	Shadow	Tree	Backg.	Shadow	Tree	Backg.	Shadow	Tree	Backg.	Shadow
CASI01_02	0.000	0.938	0.061	0.159	0.521	0.319	0.050	0.816	0.132	0.043	0.824	0.131
CASI01_06	0.041	0.936	0.022	0.092	0.509	0.397	0.102	0.660	0.236	0.094	0.465	0.440
CASI01_10	0.003	0.660	0.335	0.077	0.790	0.132	0.023	0.924	0.052	0.022	0.905	0.072
SPRINT model	0.104	0.701	0.194	0.104	0.701	0.194	0.104	0.701	0.194	0.104	0.701	0.194

Table 4. Estimated fractional covers obtained by the linear and nonlinear SVM-based models for the scenes with translucent trees and sparse population.

	Linear kernel			Polynomial kernel			RBF kernel			Sigmoid kernel		
Scene	Tree	Backg.	Shadow	Tree	Backg.	Shadow	Tree	Backg.	Shadow	Tree	Backg.	Shadow
CASI01_03	0.012	0.781	0.206	0.272	0.416	0.310	0.199	0.413	0.386	0.240	0.503	0.256
CASI01_07	0.038	0.829	0.132	0.225	0.486	0.287	0.276	0.418	0.304	0.253	0.374	0.372
CASI01_11	0.154	0.802	0.145	0.262	0.402	0.335	0.280	0.407	0.311	0.291	0.353	0.353
SPRINT model	0.294	0.383	0.318	0.294	0.383	0.318	0.294	0.383	0.318	0.294	0.383	0.318

Table 5. Estimated fractional covers obtained by the linear and nonlinear SVM-based models for the scenes with opaque trees and dense population.

	Linear kernel			Polynomial kernel			RBF kernel			Sigmoid kernel		
Scene	Tree	Backg.	Shadow	Tree	Backg.	Shadow	Tree	Backg.	Shadow	Tree	Backg.	Shadow
CASI01_04	0.202	0.602	0.195	0.211	0.458	0.330	0.276	0.257	0.365	0.107	0.618	0.273
CASI01_08	0.209	0.661	0.129	0.252	0.402	0.344	0.329	0.317	0.253	0.160	0.656	0.183
CASI01_12	0.194	0.609	0.198	0.251	0.428	0.372	0.376	0.292	0.331	0.193	0.591	0.198
SPRINT model	0.279	0.357	0.362	0.279	0.357	0.362	0.279	0.357	0.362	0.279	0.357	0.362

Table 6. Estimated fractional covers obtained by the linear and nonlinear SVM-based models for the scenes with translucent trees and dense population.

Table 3 shows the fractional covers estimated by the different spectral mixture models (linear, polynomial-based, RBF-based and sigmoid-based) for the scenes with opaque trees and sparse population, along with the SPRINT calculated fractions for the purpose of comparison. Overall, it can be noted that the polynomial and RBF-based nonlinear mixture models provide more accurate results than the linear model in this set of scenes. On other hand, Table 4 shows the results obtained by the different mixture models for the scenes with translucent trees and sparse population. In this set of

images, the polynomial-based mixture model provides the best overall results, in particular for the scene with dark background, while the RBF-based mixture model provides the most similar results to the SPRINT model for the scene with white background. Table 5 reveals that the three nonlinear mixture models tested provide results which are better than those found using the linear model for abundance estimation in the scenes with opaque trees and dense population. Finally, Table 6 shows that both the polynomial-based and RBF-based mixture models provide the most accurate fractional abundance estimation of constituent materials in the scenes with translucent trees and dense population. In this last case, the linear model and the sigmoid-based model produce similar results.

From the results in Tables 3-6, it can be deduced that the nonlinear SVM with polynomial kernel and the nonlinear SVM with RBF kernel produce results which are superior to those found using the standard linear mixture model. In addition, the two nonlinear mapping schemes above tend to produce more accurate results than those found using the nonlinear SVM with sigmoid kernel. In nonlinear mappings, the margin boundaries are no longer linear or parallel, as shown in Fig. 2, but they more closely represent the shape of the class distributions in the analyzed scenes. Given this result, it can be argued whether the linear mixture assumptions are appropriate for these scenes or not. The results shown in Tables 3-6 indicate that, when nonlinear transformations of the measured spectral bands are introduced, the performance of the nonlinear model on the mixed pixel dataset is better than the linear SVM algorithm, which is equivalent to a constrained least squares linear mixture model as reported in previous work.

5. CONCLUSIONS

In this work, we have reported on the application of nonlinear SVMs for inferring land cover fractions within hyperspectral scenes. A database of laboratory simulated-forest scenes was used to carry out a comparative analysis of the proposed techniques to the standard linear mixture model. The areal fractions of the main constituents in these scenes were calculated by the SPRINT canopy model for comparison. Our quantitative and comparative analysis yields the following conclusions: 1) The errors in the estimated fractions by the standard linear mixture model are very large; and 2) Nonlinear SVMs based on polynomial and RBF kernels outperform the standard linear mixture model, particularly in the scenes with translucent trees. As a result, this investigation suggests that nonlinear mixture models are needed to account for the multiple scattering between tree crowns and background for the simulated scenes used in this study, which accurately resemble the mixing properties which are present in a real-world scenario.

ACKNOWLEDGEMENT

We gratefully thank John R. Miller and Baoxin Hu from CRESTech for providing the laboratory simulated-forest CASI hyperspectral data used in experiments. In particular, we would like to thank John R. Miller for many helpful discussions and suggestions during a research visit to our laboratory, and also for his willingness to share the CASI data with us. Funding of this research by the Spanish Government is also gratefully acknowledged.

REFERENCES

1. N. Keshava, J.F. Mustard, “Spectral unmixing,” *IEEE Signal Processing Magazine*, vol. 19, pp. 44-57, 2002.
2. J.F. Mustard and J.M. Sunshine, “Spectral analysis for earth science investigation,” in: *Remote Sensing for the Earth Sciences*, Wiley: New York, 1999.
3. P.J. Zarco-Tejada, J.R. Miller, T.L. Noland, G.H. Mohammed, P.H. Sampson, “Scaling-up and model inversion methods with narrow-band optical indices for chlorophyll content estimation in closed forest canopies with hyperspectral data,” *IEEE Transactions on Geoscience and Remote Sensing*, vol. 39, pp. 1491-1507, 2001.
4. K.J. Guilfoyle, M.L. Althouse, C.-I Chang, "A quantitative and comparative analysis of linear and nonlinear spectral mixture models using radial basis neural networks," *IEEE Transactions on Geoscience and Remote Sensing*, vol. 39, no. 8, Aug. 2001.
5. G.A. Carpenter, S. Gopal, S. Macomber, S. Martens, C.E. Woodcock, “A neural network method for mixture estimation for vegetation mapping,” *Remote Sensing of Environment*, vol. 70, pp. 138-152, 1999.
6. V. Vapnik, *Statistical Learning Theory*. Wiley-Interscience, New York, 1998.
7. P. Martínez, P.L. Aguilar, R.M. Pérez, A. Plaza, “Systolic SOM neural network for hyperspectral image classification,” in: *Neural Networks and Systolic Array Design*, World Scientific: Singapore, 2002.

8. M. Brown, H.G. Lewis, S.R. Gunn, "Linear spectral mixture models and support vector machines for remote sensing," *IEEE Transactions on Geoscience and Remote Sensing*, vol. 38, no. 5, May 1999.
9. C.-C Chang, C.-J Lin, "LIBSVM: A library for support vector machines," Source code available online from the following URL: http://www.csie.ntu.edu.tw/~cjlin/libsvm/.
10. B. Hu, J. Wang, J.R. Miller, N.S. Goel, "On application of spectral mixture análisis in forestry: I. Study of nonlinear mixture effects using image data analysis and SPRINT scene modeling on laboratory simulated-forest scenes," *Remote Sensing of Environment* (under review).
11. N.S. Goel and R.L. Thompson, "A snapshot of canopy reflectance models and a universal model for the radiation regime," *Remote Sensing Reviews*, vol. 18, pp. 197-225, 2000.